Fermi National Accelerator Laboratory

FERMILAB-Conf-94/345-E
E-665

# Recent Results from E665

Ashutosh V. Kotwal
Representing the E665 Collaboration
*Fermi National Accelerator Laboratory*
*P.O. Box 500, Batavia, Illinois 60510*

*Department of Physics, Harvard University,*
*Cambridge, MA 02138*

September 1994

Plenary talk presented at *VIth Rencontres de Blois, 'The Heart of the Matter' Conference,*
Blois, France, June 20-25, 1994

## Disclaimer

# RECENT RESULTS FROM E665

Ashutosh V. Kotwal
*Department of Physics, Harvard University,*
*Cambridge, MA 02138, U.S.A.*
Representing the Fermilab E665 Collaboration.

## ABSTRACT

Preliminary measurements of the structure functions $F_2^p$ and $F_2^d$, and the structure function ratio $F_2^n/F_2^p$, in inelastic $\mu N$ scattering are presented. Preliminary results on nuclear transparency $(\sigma^A/A)/\sigma^H$ in incoherent exclusive $\rho$ production are also presented. The data were obtained by Fermilab experiment 665 using a 465 GeV muon beam and liquid hydrogen, deuterium and carbon, calcium and lead targets. The structure functions are measured in the range $x_{Bj} > 8 \times 10^{-4}$ and $Q^2 > 0.2\ GeV^2$. The structure function ratio is presented as a function of $x_{Bj}$ for $x_{Bj} > 10^{-6}$. The nuclear transparency in exclusive $\rho$ production is studied as a function of $Q^2$ in the range $0.1 < Q^2 < 10.0\ GeV^2$.

## 1. Introduction

Fermilab experiment 665 is currently the highest-energy muon scattering experiment in the world. The experiment took data in the 1987-88, 1990 and 1991-92 fixed-target runs.

The experimental apparatus has been described elsewhere[1] . It consists of a beam spectrometer, an open geometry forward spectrometer, and a muon detector. The momentum resolution $\sigma(1/p)$ of the beam spectrometer is $\sim 0.8 \times 10^{-5}$ $(\mathrm{GeV/c})^{-1}$ and that of the forward spectrometer is $\sim 2 \times 10^{-5}$ $(\mathrm{GeV/c})^{-1}$ . The detector has been used for muon cross-section and cross-section ratio studies and hadronic final state studies.[2] The latter include measurements of the inclusive hadron distributions, energy flow and jet production, neutral strange particle production, and vector meson production. The nuclear dependence of the above processes has also been studied. In this presentation some of the more recent results from E665 will be discussed. These will include the measurements of the proton and deuteron structure functions, the neutron to proton structure function ratio, and the nuclear dependence of exclusive $\rho$ production.

The data used for the structure function and the structure function ratio measurements are from the 1991-92 run. A muon beam of mean energy 465 GeV impinged on cryogenic liquid hydrogen and deuterium targets, and on an evacuated vessel. The 1990 data are used for the study of nuclear dependence of $\rho$ production. In this run, carbon, calcium and lead targets were used in addition to the liquid hydrogen and deuterium targets. The mean beam energy in the 1990 run was 470 GeV. The various targets were cycled into the beam with a frequency of approximately once per minute. This procedure greatly reduces the systematic uncertainty in the ratio measurements, due to the cancellation of time-dependent corrections. The empty target data are used to subtract the contribution of the out-of-target scatters on a statistical basis.

The trigger system includes two kinds of muon triggers, the small angle trigger (SAT), and the set of large angle triggers (LAT). In addition a trigger (CAL) based on the calorimeter signals was available. The small angle trigger used a floating veto so that it could also trigger on events where the scattered muon remained within the phase space of the beam. The trigger acceptance extended to scattering angles as small as 1 mrad. The large angle triggers used veto counters in conjunction with wide angle muon detectors, providing acceptance for scattering angles above 3 mrad.

## 2. Structure Functions $\mathbf{F_2^p}$ and $\mathbf{F_2^d}$

In the single photon exchange approximation the double differential cross-section for lepton-nucleon scattering can be written as

$$\frac{d^2\sigma_{1\gamma}}{dQ^{-2}d(lnx)} = 4\pi\alpha_{em}^2 F_2(x,Q^2)[1-y-\frac{Mxy}{2E}+\frac{y^2(1+4M^2x^2/Q^2)}{2(1+R(x,Q^2))}] \qquad (1)$$

where $E$ is the incoming lepton energy, and $-Q^2$ is the square of the 4-momentum transferred from the lepton. In the lab frame $\nu$ is the lepton energy loss, $x = Q^2/2M\nu = x_{Bj}$ is the Bjorken scaling variable, and $y = \nu/E$. $\alpha_{em}$ is the electromagnetic coupling constant and $M$ is the nucleon mass. $F_2(x,Q^2)$ is the structure function of the target nucleon and $R(x,Q^2)$ is the ratio of the longitudinal to the transverse virtual photon cross-sections.

The behavior of the structure function $F_2$ is expected to be different in the small and large $Q^2$ limits. The limit $Q^2 \to \infty$ ( Deep Inelastic Scattering - DIS ) is typically understood in the infinite momentum frame. In this framework one expects scattering off point-like partons to dominate the total cross-section, and scale-independent structure functions depending only on $x_{Bj}$ are predicted. This 'Bjorken Scaling' behaviour is modified by radiative processes predicted by Quantum Chromodynamics (QCD). The struck partons are expected to be quarks that

radiate gluons and gluons that split into $q\bar{q}$ pairs. The QCD radiation causes the partons to appear at lower momentum, causing a 'pile-up' of partons at low $x_{Bj}$. Thus the structure function is expected to increase as $x_{Bj}$ falls. An explicit scale dependence is introduced through the propagators in the radiative Feynman diagrams, the phase space for the radiated partons, and perhaps the running of the strong coupling constant.

In the QCD-improved parton model, photon-nucleon scattering at lower $Q^2$ may have a significant contribution from 'higher-twist' effects in addition to the QCD radiative effects. Higher twist terms may formally be defined as terms inversely proportional to increasing powers of $Q^2$ in an expression for the photon-nucleon cross-section. These terms correspond to the photon scattering off multi-parton states in the proton. Another way to interpret these processes is that the struck parton interacts with other partons in the proton.

Apart from the QCD-improved parton model, the photon-nucleon scattering process has also been described in the nucleon rest frame. Since the photon couples to hadrons, the physical photon can be considered as a mixture of a 'bare' photon and a hadronic state. At high energies, a low-mass hadronic state becomes almost degenerate with the 'bare' photon in energy, so that it can become a large component of the physical photon. The photon-nucleon scattering then occurs mainly due to the interaction of the hadronic component of the photon with the nucleon. Furthermore, the Vector Meson Dominance (VMD) model states that the spectrum of the hadronic component is dominated by the low mass vector mesons. The Generalized Vector Meson Dominance (GVMD) model includes the contribution of higher mass states.

In the photoproduction limit, $\lim_{Q^2 \to 0} F_2 = \sigma_{\gamma N} Q^2 / 4\pi^2 \alpha$, where the factor of $Q^2$ is obtained from gauge invariance and $\sigma_{\gamma N}$ is the real photon-nucleon cross-section. The scaling photon-nucleon cross-section would vary as the inverse square of energy. However, measurements show that $\sigma_{\gamma N}$ increases slowly with energy at high energies, in a manner similar to the measured hadron-hadron cross-sections. This supports the premise that at high energies, photon-hadron interactions are mediated by the hadronic component of the photon.

Thus we have different expectations of the structure function in the high and low $Q^2$ limits. In the former case we expect approximate scaling due to point-like photon-parton interactions, with an increase at low $x_{Bj}$ and logarithmic scale dependence introduced by QCD radiative effects. In the latter case, the vector dominance model explains the structure function in terms of the hadronic components of the photon, resulting in non-scaling behaviour and only a weak $x_{Bj}$ dependence at fixed $Q^2$. Historically, it was realized that the application of GVMD at high $Q^2$ would continue to predict non-scaling behaviour, leading to an inconsistency with Bjorken Scaling.[3] This inconsistency was resolved when it was realized that Bjorken Scaling resulted from the photon's coupling to point-like quarks. Hence, in GVMD, the high mass hadronic components of the photon would correspond to highly virtual $q\bar{q}$ states, corresponding to spatially small color dipoles. The dipole field would reduce as the dipole shrinks with increasing $Q^2$, resulting in a diminishing cross-section with the nucleon. This is the idea of the 'shrinking-photon' or 'color-transparency', which restores the scaling behaviour of the structure function at high $Q^2$ in GVMD.

The measurement of the structure function extending from low to high $Q^2$ can help to illuminate the transition in the photon-nucleon scattering mechanism between these limits. This measurement from the E665 data is described in this section. The nuclear dependence of exclusive $\rho$ production offers a way to look for an explicit signal of color transparency. This measurement will be described in a following section.

In order to extract the structure function from the event rates, the absolute luminosity, radiative corrections and apparatus effects must be known. The apparatus acceptance, trigger and reconstruction efficiencies, and smearing corrections are calculated using data and Monte Carlo studies. The absolute luminosity is calculated by measuring the length, temperature and

pressure of the liquid targets, and counting the number of beam muons. The total beam count is maintained by scalers, while a randomly prescaled version of the beam signal is used to provide beam triggers. The measurement can be made insensitive to various experimental losses of luminosity by normalizing the physics triggers (which require the beam signal in coincidence) to the number of beam triggers off-line.

The experimentally measured quantity is the total muon double differential cross-section. In order to extract $F_2$, electromagnetic radiative corrections must be applied, and $R$ must be known. For the analysis presented here, radiative corrections are calculated by the computer program FERRAD35[4] according to the formulation of Mo and Tsai.[5] The input $F_2$ is constructed from published fits[6–8] to SLAC, DESY, Daresbury and NMC data and the low $Q^2$ interpolation at high $W^2$ of Donnachie and Landshoff.[9] $R$ is taken as $R_{slac}$.[10] The $H_2$ and $D_2$ event rates are corrected and normalized using an event-by-event weighting procedure.

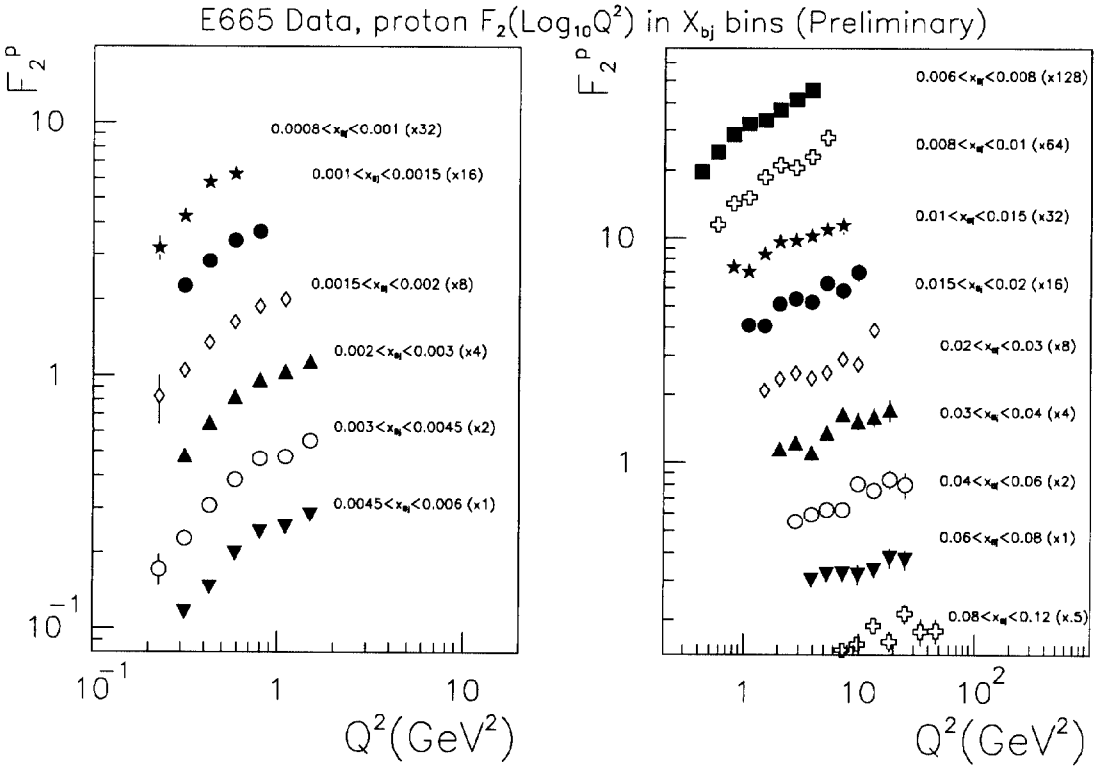


Fig. 1. $F_2^p$ as a function of $Q^2$ in $x_{Bj}$ bins.The errors shown are statistical.

Events used for the structure function measurement are required to have the beam energy between 350 and 600 GeV, $\nu > 25$ GeV and the energy of the scattered muon greater than 80 GeV. SAT events are used for the analysis. The kinematics of the event are determined from the 4-momenta of the beam and the scattered muon at the reconstructed vertex. The data sample consists of 664 nb$^{-1}$ of $\mu p$ data and 749 nb$^{-1}$ of $\mu d$ data.

The $F_2$ results for the proton are shown in figure 1. The errors shown are statistical only. The systematic uncertainty is of the order of 10-20%. This includes uncertainties in the luminosity of ~1%, trigger efficiency ~5-10% and reconstruction efficiency ~10-15% respectively. The maximum radiative correction is ~45% and agrees with the calculation[11] using the method of Bardin et. al. to ~2%. The difference between $F_2$ obtained using $R_{QCD}$ and $R_{slac}$ is a few percent at low $x_{Bj}$ and high $y$ and smaller elsewhere. The results for the deuteron $F_2$ are similar. The results are preliminary and the systematic uncertainty is expected to reduce as the analysis progresses.

The measurement covers the range $8\times10^{-4} < x_{Bj} < 0.12$ and $Q^2 > 0.2$ GeV$^2$. The $x_{Bj}$ values are comparable to those obtained at HERA and extend to lower values than those achieved at previous fixed target experiments. The $Q^2$ range extends from the regime of perturbative QCD at high $Q^2$ down to low $Q^2$ values where $F_2$ has a strong $Q^2$ dependence approaching the photoproduction limit. The $x_{Bj}$ dependence of $F_2$ is weak at low $Q^2$, as shown in figure 2.

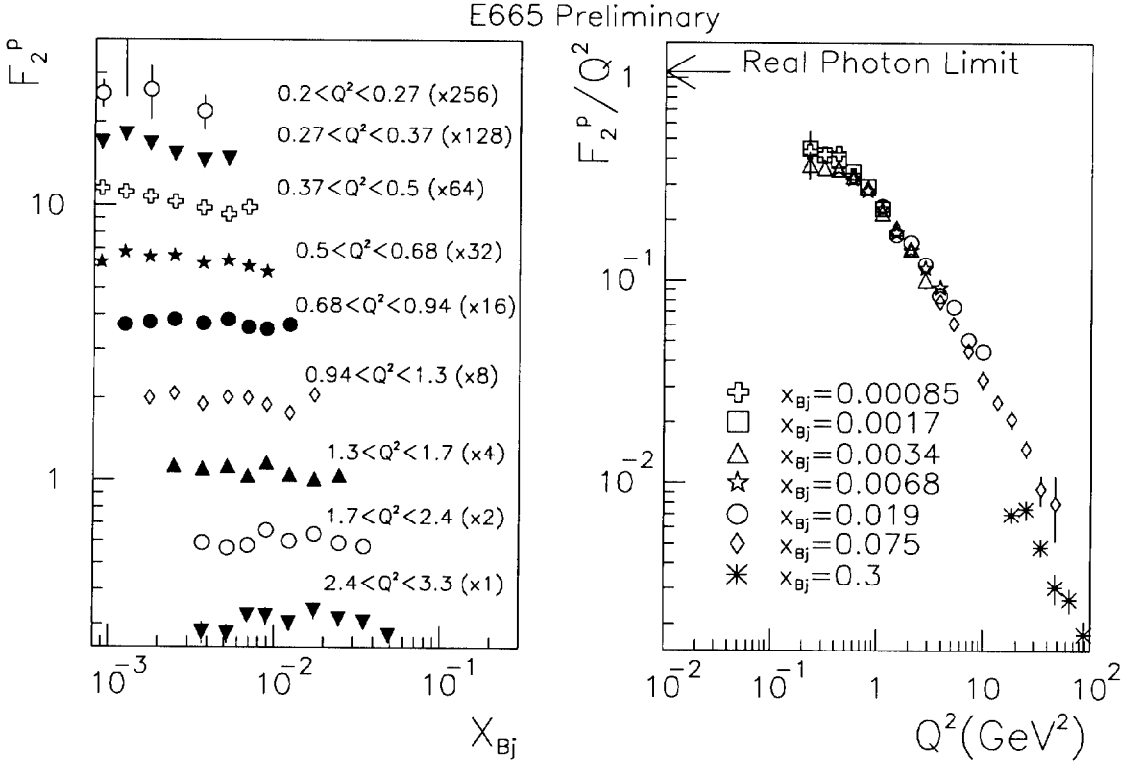


Fig. 2. $F_2^p$ vs $x_{Bj}$ for different $Q^2$, and $F_2^p/Q^2$ vs $Q^2$ for different $x_{Bj}$.

## 3. Structure Function Ratio $F_2^n/F_2^p$

The neutron cross-section is assumed to be the difference of the deuteron and the proton cross-sections. In the parton model with the assumption of sea isospin symmetry, the neutron-to-proton structure function ratio is expected to approach unity as $x_{Bj} \to 0$. One can obtain a prediction for the value of the Gottfried integral to be 1/3, where the Gottfried integral $S_G = \int_0^1 (F_2^p - F_2^n) dx_{Bj}/x_{Bj}$. Therefore it is interesting to measure the structure function ratio at low $x_{Bj}$. Regge phenomenology also predicts that $F_2^p - F_2^n$ should behave as $\sqrt{x_{Bj}}$ at low $x_{Bj}$.

However, the measurement is made with deuterons and not with free neutrons. One might expect nuclear effects in the deuteron, leading to shadowing in the deuteron with respect to the proton. These effects may be anticipated due to the hadronic nature of the photon at low $Q^2$, or due to recombination of partons from different nucleons. Hence one is motivated to measure the deuteron-to-proton cross section ratio at low $x_{Bj}$ and $Q^2$ where these effects are likely to manifest themselves.

For the extraction of the ratio the following cuts are made on the $H_2$ and $D_2$ data samples: $0.1 < y < 0.8$, $\nu > 40$ GeV, $\delta\nu/\nu < 0.3$, $Q^2 > 0.1$ GeV$^2$ (SAT) or $Q^2 > 0.001$ GeV$^2$ (CAL), and 350 GeV $< \nu <$ 600 GeV.

Three different methods are used to extract the structure function ratio, each method giving the best result in a different range of $x_{Bj}$. In the first method, SAT data are used and radiative corrections are applied to the ratio $\sigma_n/\sigma_p$, in a manner similar to the absolute $F_2$

measurement. This method is restricted to the range $x_{Bj} > 8 \times 10^{-4}$ to avoid the muon-electron elastic scattering contamination peaking at $x_{Bj} = m_e/m_p = 0.000545$.

The second method uses the electromagnetic (EM) calorimeter to identify and remove the $\mu - e$ elastic scatters and hard muon bremsstrahlung events. It uses the properties that (*i*) the production angles involved in these events are typically small, and (*ii*) all the energy loss is electromagnetic and hence is detected in the calorimeter. The spatial spread of the energy deposited in the calorimeter (should be small), and the energy of the largest calorimeter cluster normalized to $\nu$ (should be large) are used to identify electromagnetic background events. The SAT events surviving the cut are used to measure $\sigma_n/\sigma_p$, and extend the measurement from the SAT data down to the lowest available $x_{Bj}$ of $10^{-4}$.

The third method uses the calorimeter trigger data, which extends down to $x_{Bj} > 10^{-6}$ since the trigger makes no minimum muon scattering angle requirements. The trigger is constructed such that only the signals produced in the outer regions of the calorimeter are used to define the trigger. Some vertical and horizontal spread in the calorimeter energy flow is required. This construction selects hadronic event topologies and is very efficient at rejecting $\mu e$ and hard muon bremsstrahlung events.

The neutron to proton structure function ratio $F_2^n/F_2^p$ is directly related to the single photon exchange cross-section ratio $\sigma_n/\sigma_p$ if $R^p$ is assumed to be equal to $R^n$ (the $R$ difference is measured[10] to be consistent with zero in part of the kinematic range covered by this measurement). The ratio $\sigma_n/\sigma_p$ is shown in figure 3 for the three techniques, each being shown where it has the smallest systematic error. The results from the three methods are consistent with each other in the regions of their respective overlaps. The error bars shown are statistical only. The total systematic uncertainty is less than 3.5%, including uncertainties in the relative normalization, trigger acceptance and the effect of analysis cuts. These uncertainties are determined from the data using monitoring triggers and Monte Carlo studies.

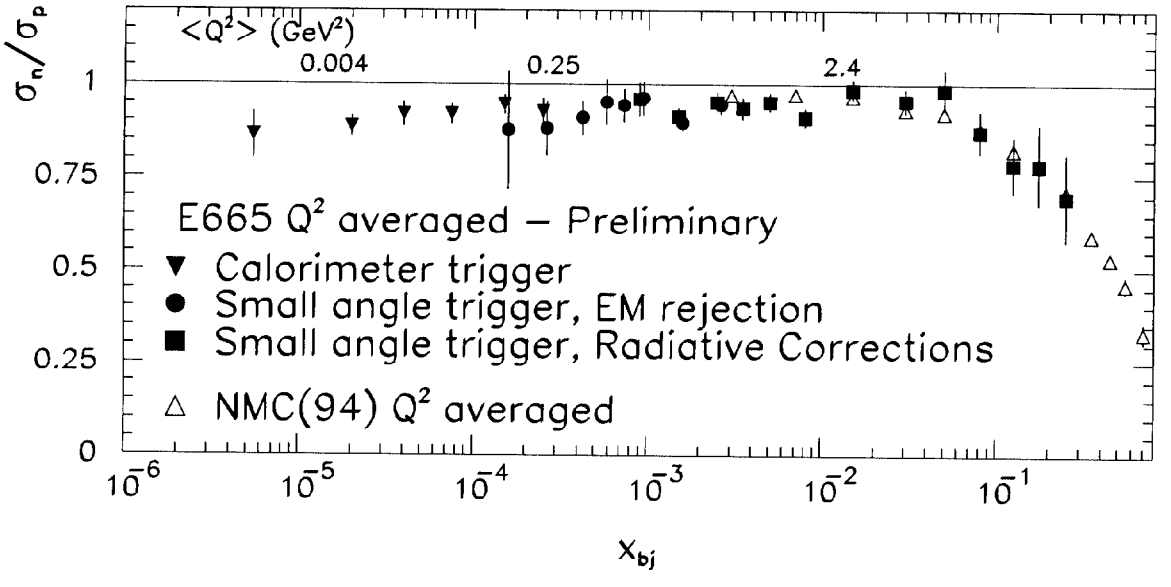


Fig. 3. $\sigma_n/\sigma_p$ as a function of $x_{Bj}$ . Also shown are results from the CERN NMC experiment.[14]

The data in the different $x_{Bj}$ bins cover different ranges of $Q^2$. The average $Q^2$ for the $x_{Bj}$ values of $5 \times 10^{-6}$, $2 \times 10^{-4}$ and $1.5 \times 10^{-2}$ is shown. The result from the NMC data re-analysis[14] is also shown. There is good agreement in the region of overlap, while the E665 measurement extends three decades lower in $x_{Bj}$.

The average value of the ratio is $\sim 0.94$ for $x_{Bj} < 0.05$. The deviation from unity may be due to shadowing and is consistent with model calculations of shadowing in the deuteron.[12,13] Using the model[12] to correct the deuteron data, can reduce the Gottfried integral by 10-15% compared to the value extracted without shadowing corrections.[14] The measurement may also be interpreted as a difference in the proton and neutron structure functions. If this is the case then, using the measured $Q^2$ dependence (figure 4) to extrapolate the ratio to $Q^2 = 4$ GeV$^2$, the Gottfried integral gets a positive contribution of $\sim 0.05$ per decade in $x_{Bj}$, down to $x_{Bj} \sim 10^{-4}$.

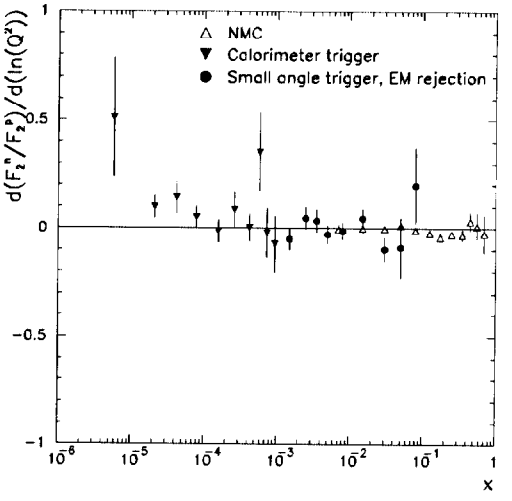


Fig. 4. Slope of $\sigma_n/\sigma_p$ with respect to $lnQ^2$ as a function of $x_{Bj}$ . Also shown are results from the CERN NMC experiment.[14]

## 4. Nuclear Transparency in Exclusive $\rho$ Production

A model for the muo-production of exclusive $\rho$ can be described as follows. The virtual photon radiated by the muon fluctuates into a 'virtual $\rho$', which is a $q\bar{q}$ state. This state has a color dipole moment which is inversely proportional to $\sqrt{Q^2}$, and a coherence length given by $l_c \sim 2\nu/(Q^2 + M^2)$, where $M$ is the invariant mass of the $q\bar{q}$ state. The 'virtual $\rho$' interacts with the target nucleon or nucleus elastically, exchanging some 4-momentum whose square is denoted by $t$. Following the scatter, the 'virtual $\rho$' reverts to a normal $\rho$ with a formation length $l_f \sim \nu/(m\Delta m)$, where $m$ is the mass of the $\rho$ and $\Delta m$ is the typical mass splitting for vector mesons. It is detected as an exclusive $\rho$ through its decay to two charged pions carrying all the energy lost by the muon (within kinematic bounds and experimental resolution). Specifically, the final state nucleon or nucleus is not detected.

At low $Q^2$, the 'virtual $\rho$' has a large color dipole moment and undergoes strong hadronic re-interactions. This leads to suppression of exclusive $\rho$ production for nuclear targets with respect to the proton. At high $Q^2$, the 'virtual $\rho$' is a smaller dipole with a weaker color field. Therefore the nucleus tends to become 'color transparent' to the 'virtual $\rho$' and the initial and final state reinteractions of the $\rho$ are reduced. This causes the nuclear suppression to vanish as the dipole moment reduces.

If the experimentally measured nuclear transparency, defined as the ratio of per-nucleon cross-sections for a nucleus (mass number $A$) with respect to hydrogen, can be parametrized as $(\sigma^A/A)/\sigma^H \sim A^{\alpha-1}$, then the signal for color transparency is that $\alpha$ is observed to increase with $Q^2$, tending to unity at high $Q^2$.

For this signal to appear, it is necessary that the 'virtual $\rho$' state survive long enough to propagate through the nucleus before appearing as the normal state. The large boost available at E665 ($< \nu > \sim$ 120 GeV) causes the coherence and formation time to be Lorentz-dilated so that this criterion is fulfilled.

Exclusive $\rho$ events are selected from SAT and LAT events in the following manner. One positive and one negative track, in addition to the scattered muon, are required to be fitted to the muon-muon vertex. No other tracks should be detected. The number of unused vertex drift chamber hits are required to be consistent with the absence of other charged particles. The hadron energies are required to be greater than 10 GeV each to ensure good reconstruction. Photon conversions are removed by using the calorimeter to identify electron tracks and requiring the two-electron invariant mass $M_{e^+e^-} > 0.5$ GeV. $\phi$ mesons are removed by requiring the two-kaon invariant mass $M_{K^+K^-} > 1.05$ GeV. Events are required to have $\nu > 20$ GeV and $\delta\nu/\nu < 0.25$ to ensure good resolution on $\nu$.

Following this selection, the variable $z_\rho$ is studied, where $z_\rho$ is the sum of the two hadron energies normalized to $\nu$. For exclusive $\rho$ events in which the recoiling target carries very little energy, $z_\rho$ is expected to be unity within experimental resolution. Therefore one expects a peak at zero with a width of unity in the variable $(z_\rho - 1)/\delta z_\rho$ , where $\delta z_\rho$ is the calculated error on the reconstructed $z_\rho$. As shown in figure 5, we indeed find the expected peak, with a tail extending to lower values of $(z_\rho - 1)/\delta z_\rho$. This tail can be caused by radiative and background processes that satisfy the analysis cuts. The contribution of the tail under the peak is estimated from a DIS Monte Carlo sample normalized to the tail. The final exclusive $\rho$ sample is obtained by making the cut $-1.5 < (z_\rho - 1)/\delta z_\rho < 3$.

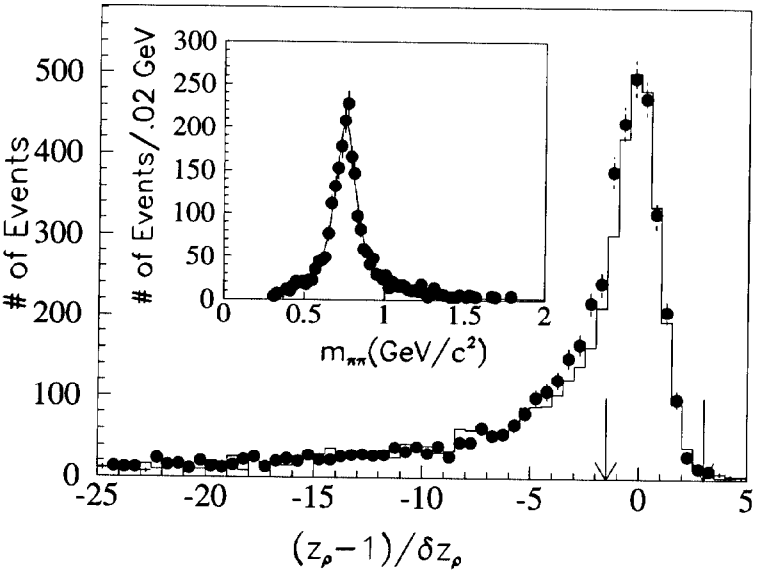


Fig. 5. The deviation of $z_\rho$ from unity normalized to $\delta z_\rho$. The circles show the data, and the solid histogram shows the Monte Carlo obtained by combining appropriate amounts of DIS and exclusive $\rho$ Monte Carlo samples. The arrows indicate the cut used to select exclusive $\rho$. The insert shows the two-pion invariant mass distribution for the selected events, along with the fitted curve.

The insert in figure 5 shows the $\pi\pi$ invariant mass for the selected events. The distribution is fitted with a $P$-wave Breit-Wigner function with a phenomenological mass skewing factor. The fit gives parameters that are reasonably close to the Particle Data Group values. Figure 6 shows the $t'$ distribution for calcium and hydrogen, where $t' = t - t_{min}$ and $t_{min}$ is the minimum $t$ required by energy-momentum conservation when the $\rho$ is collinear with the virtual photon. The $t'$ distribution can be described by two exponentials, a steep coherent component at small $t'$

and a flatter incoherent component extending to larger values of $t'$. The slope of the incoherent component is similar for all targets, as expected for production off individual nucleons. The slope $b_A$ of the coherent component (fitted with the form $e^{-b_A|t'|}$) is observed to behave as $b_A \sim A^{2/3}$, as expected for production off the whole nucleus.

The incoherently produced $\rho$ are selected by requiring $t' > 0.1$ GeV$^2$, beyond which there is negligible contribution from the coherent component. Figure 7*a* shows the measured nuclear transparency $T = (\sigma^A/A)/\sigma^H$ as a function of A, in three $Q^2$ bins. In each $Q^2$ bin the data fitted to the form $T \sim A^{\alpha-1}$ give good $\chi^2$. From the fitted slopes, the parameter $\alpha$ is obtained, and is shown as a function of $Q^2$ in figure 7*b*. The error bars are statistical. Studies have shown that the systematic uncertainties are negligible. The data show that $\alpha$ increases with $Q^2$ and approaches unity at high $Q^2$. This is consistent with a signal of color transparency. The $\chi^2$ probability is 2% that $\alpha$ is independent of $Q^2$.

## 5. Summary

Preliminary measurements of the structure function $F_2$ in the range $x_{Bj} > 0.0008$ and $Q^2 > 0.2$ GeV$^2$ are presented. At low $Q^2$, $F_2$ falls rapidly with $Q^2$ with a slope approaching the photoproduction limiting value. There is little $x_{Bj}$ dependence at low $x_{Bj}$. At higher $Q^2$, $F_2$ has milder variation with $Q^2$ and it increases as $x_{Bj}$ reduces. This behaviour suggests that the photon makes a transition from being a hadron-like object at low $Q^2$ to a point-like probe at high $Q^2$ where perturbative QCD is applicable.

Preliminary results on the neutron-to-proton cross-section ratio $\sigma_n/\sigma_p$ are presented in the range $x_{Bj} > 10^{-6}$ and $Q^2 > 0.001$ GeV$^2$. The average value of the ratio is below unity ( $0.94 \pm 0.01$(stat)$\pm 0.035$(syst) ) for $x_{Bj} < 0.05$, and is consistent with model calculations of shadowing in the deuteron.[12,13] There is no evidence for a significant $Q^2$ dependence of the ratio.

Preliminary results on nuclear transparency in exclusive $\rho$ production are presented. Increase in the nuclear transparency $(\sigma^A/A)/\sigma^H$ with $Q^2$ is observed in the incoherent production channel, in a manner consistent with the idea of color transparency.

## References


1. M.R. Adams, et.al., *Nucl. Inst. Methods* **A291** (1990) 533.
2. M.R. Adams, et.al., *Phys. Lett.* **B272** (1991) 163; *Phys. Lett.* **B287** (1992) 375; *Phys. Rev. Lett.* **68** (1992) 3266; *Phys. Rev. Lett.* **69** (1992) 1026; *Phys. Rev.* **D48** (1993) 5057; *Phys. Lett.* **B308** (1993) 418; *Phys. Lett.* **B309** (1993) 477; *Z. Phys. C* **61** (1994) 179; *Z. Phys. C* **61** (1994) 539; *Phys. Rev.* **D50** (1994) 1836; *Phys. Rev. Lett.* **72** (1994) 466;
3. T. H. Bauer, R. D. Spital, D. R. Yennie and F. M. Pipkin, *The hadronic properties of the photon in high-energy interactions,* Reviews of Modern Physics, Vol. 50, No. 2, April 1978
4. P. Amaudruz, et.al., *Nucl. Phys.* **B273** (1992) 3.
5. L.W. Mo and Y.S. Tsai, *Rev. Mod. Phys.* **41** (1969) 205.
6. F. W. Brasse et. al. *Nucl. Phys.* **B39** (1972) 421-431.
7. F. W. Brasse et. al. *Nucl. Phys.* **B110** (1976) 413.
8. New Muon Collaboration, *Phys. Lett.* **B295** (1992) 159-168.
9. A. Donnachie and P.V. Landshoff, *Z. Phys.* **C61** (1994) 139.
10. L.W. Whitlow, et.al, *Phys. Lett.* **B250** (1990) 193.
11. B. Badełek, et. al. Preprint TSL/ISV-94-0092
12. B. Badełek, J. Kwieciński, Preprint TSL/ISV-93-0090
13. W. Melnitchouk, A. W. Thomas, *Phys. Lett.* **B317** (1993) 437.
14. NMC Collaboration, Preprint CERN-PPE/94-32

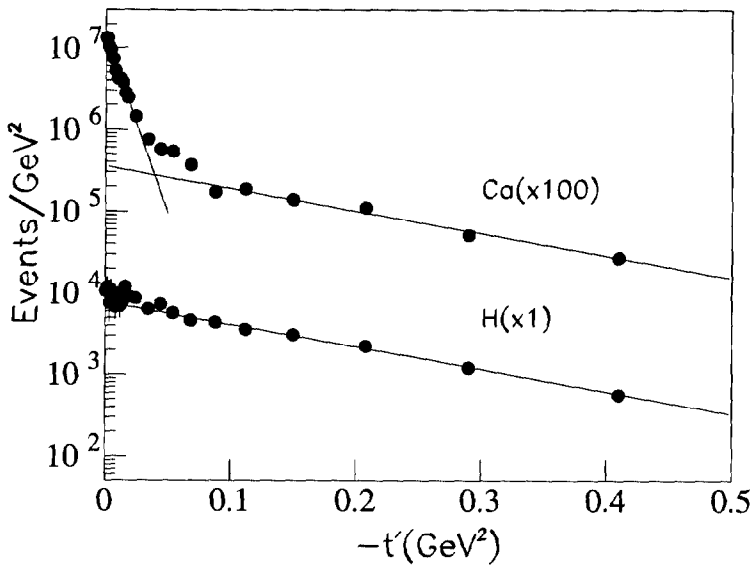


Fig. 6. $t'$ distributions for calcium and hydrogen.

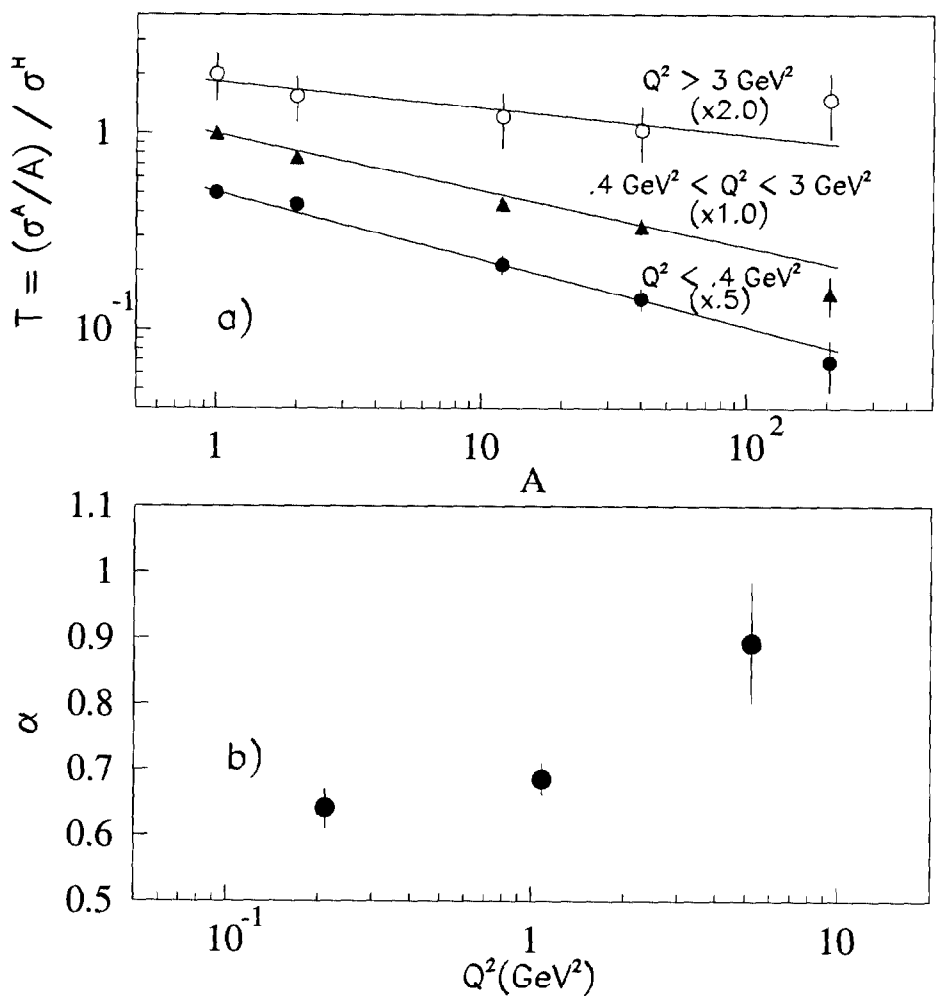


Fig. 7. ($a$) Nuclear transparency versus atomic mass number in various $Q^2$ bins, for incoherent exclusive $\rho$ production. Fits were performed to the form $A^{\alpha-1}$. ($b$) $\alpha$ vs $Q^2$ with statistical errors.